metals

MDPI

Article

# Effects of CaO Addition on the Iron Recycling from Nickel Slags by Oxidation-Magnetic Separation

**Yongbo Ma [1,2] and Xueyan Du [1,2,*]**

[1] State Key Laboratory of Advanced Processing and Recycling of Non-Ferrous Metals, Lanzhou University of Technology, Lanzhou 730050, China; mark62534@sina.com
[2] School of Materials Science and Engineering, Lanzhou University of Technology, Lanzhou 730050, China
* Correspondence: duxy@lut.cn; Tel.: +86-931-297-3961

Received: 31 October 2018; Accepted: 14 November 2018; Published: 16 November 2018


**Abstract:** To recover iron from water-quenched nickel slags, CaO was added. Thermodynamic analysis showed that CaO promotes the reaction between fayalite ($Fe_2SiO_4$) and $O_2$. Phase diagrams of the FeO-$SiO_2$-MgO-CaO slag with various CaO contents in an air atmosphere drawn by FactSage 7.1 showed that the phase components can be significantly affected by the CaO contents. With increasing CaO content, the fusion characteristic temperatures decreased rapidly to a minimum and subsequently increased slightly. The oxidization of $Fe_2SiO_4$ in nickel slags was accelerated significantly by the addition of CaO, which led to an increase of FeO activity and decrease of $Fe_2O_3$ activity to promote the formation of $MgFe_2O_4$. Excess addition of CaO led to the formation of more silicates. In addition, the crystallization temperature was also reduced with increasing CaO content, causing less spinel to crystalize. With increasing CaO content, the iron recovery and yield of concentrate first increased and subsequently decreased, while the total iron (TFe) content was almost not influenced and maintained a relatively stable value.

**Keywords:** nickel slag; fusion temperature; oxidization; crystallization temperature; magnetic separation

## 1. Introduction

More than 1.6 million tons of nickel slags are produced annually by Jinchuan Nonferrous Metals Company (JNMC), the 4th largest nickel manufacturer in the world, most of which are landfilled. This iron-rich slag contains appropriately 40 wt.% iron, as well as high-value metals such as Ni, Co and Cu. Therefore, utilization of nickel slag is indispensable for the sustainable growth of the nickel industry, especially when iron ore is deficient in China, about 70% of which is imported. As reported previously [1–3], fayalite is the dominant iron-containing phase in water-quenched nickel slags. Due to some stubborn disadvantages [4–6], the reduction-magnetic separation has not been industrially applicated yet in China after an industrial experiment performed in 1994 [7], where nickel slag was used for the production of weathering steel (12MnCuCrNi). An environmentally friendly method, the oxidization-magnetic separation [5], was presented for iron recycling in the form of magnetic iron oxides ((Fe,Mg)$Fe_2O_4$). However, the results showed that iron recycling by both methods can be significantly improved by the appropriate addition of CaO, suggesting that the addition of CaO is beneficial for iron recycling from iron-rich nickel slags.

As a cheap flux with strong alkality, CaO is widely used in the metallurgical industry as a flux that is superior to other alkaline oxides, such as MgO, MnO, and $Na_2O$. Results showed that the addition of CaO can influence the slag in many aspects. Ducret and Rankin [8] found that CaO caused a moderate decrease in the liquidus temperature. Using semi-empirical results in our previous study [5], the qualitative conclusion was drawn that the fusion temperature can be influenced by the addition of CaO.

Fujino et al. [9] found that the liquidus temperature at the contact points between CaO particles and magnetite produced on wüstite particles was reduced by the addition of CaO. Mackwell [10] reported that the products of the oxidization of single crystal samples of the synthetic fayalite consisted of $Fe_3O_4$, $Fe_2O_3$, and $SiO_2$. When studying the kinetics of the oxidation of divalent iron to trivalent state in liquid FeO-CaO-$SiO_2$ slag, Semykina et al. [11] found that the products consisted of $Fe_2O_3$, $Fe_3O_4$, and $CaSiO_3$ at 1773 K, while $Ca_2Fe_2O_5$ was also formed during oxidation at 1673 K. However, the oxidation kinetics of the liquid FeO-MnO-CaO-$SiO_2$ slag in air were also investigated by Semykina [12], who found that the products were $MnFe_2O_4$, $Fe_3O_4$, $CaSiO_3$, and $Ca_3Si_2O_7$. Heo et al. [13] found that the $Fe^{3+}/Fe^{2+}$ ratio in the slag at a fixed temperature could be affected by changing the composition when free $O^{2-}$ ions were presented due to the addition of basic oxides, such as CaO. To recover iron from copper smelting slag using carbon, Heo et al. [14] also found that the iron recovery could be increased by the addition of CaO if the CaO content was less than 20 wt.% but rapidly decreased when the CaO content was 30 wt.%. FactSage 6.3 was used by Heo et al. [14] to investigate the influence of CaO addition on the mass fraction of solid phases, results showed that the solid phase cannot be precipitated only at 20 wt.% CaO after reduction for 60 min at 1773 K, indicating that the crystallization temperature of the phases can be affected by the addition of CaO. The effects of CaO on the precipitation morphology of metallic iron during the reduction of iron oxides under a CO atmosphere were investigated by Zhao et al. [15], who found that whisker formation of reduced iron can be promoted by a CaO content of less than 4 wt.%, but no whiskers were observed if the content was more than 8 wt.%.

Therefore, the effects of CaO addition on the fusion characteristic, oxidation, crystallization, and magnetic separation were investigated in the present work.

## 2. Materials and Methods

### *2.1. Materials*

The chemical compositions of water-quenched nickel slags, acquired from a nickel flash furnace in JNMC, are presented in Table 1. Fayalite was identified as the dominant phase in the iron-rich slag in our previous work [5].

**Table 1.** Chemical composition of water-quenched nickel slag (wt.%).

| TFe | Si | Mg | Ca | S | Ni | Co | Cu | Pb | Zn | As |
|---|---|---|---|---|---|---|---|---|---|---|
| 36.22 | 14.28 | 8.94 | 3.75 | 0.63 | 0.65 | 0.12 | 0.27 | 0.001 | 0.043 | 0.001 |

Calcium oxide (CaO) powder with a purity of 98.0%, supplied by Tianjin Baishi Chemical Industry Co. Ltd. (Tianjin, China), was added to adjust the content of CaO in the slag samples. Argon with a purity of 99.999% was supplied by Xi'an Teda Cryogenic Equipment Co. Ltd. (Xi'an, China).

### *2.2. Equipment*

FactSage 7.1 (FACT, Montreal, Quebec, Canada; GTT Technologies, Aachen, Germany) was used for thermodynamic calculations. The measurements of the fusion characteristic temperatures were performed by a hot stage microscope (HSM, LZ-III, Northeastern University, Shenyang, China) shown schematically in Figure 1. A horizontal furnace (HTL-1700-80, Shanghai Haoyue Electric Technology Co. Ltd., Shanghai, China) with an alumina tube (80 mm dimeter and 1000 mm length) was used for sample heating and controlling the temperature. Rectangular alumina boats for holding the slags were 99.99% pure with lengths of 90 mm, widths of 60 mm, heights of 20 mm, and thicknesses of 1 mm. A grinder (GJ-400-1, YongSheng mineral equipment manufacturing Co. Ltd., Ganzhou, China) was used for sample crushing. A wet feebleness magnetic-separation machine (XCGQ-50, Tangshan Shida automation instrumentation technology Co. Ltd., Tangshan, China) with a maximum magnetic flux density of 350 mT was used for the magnetic separation.

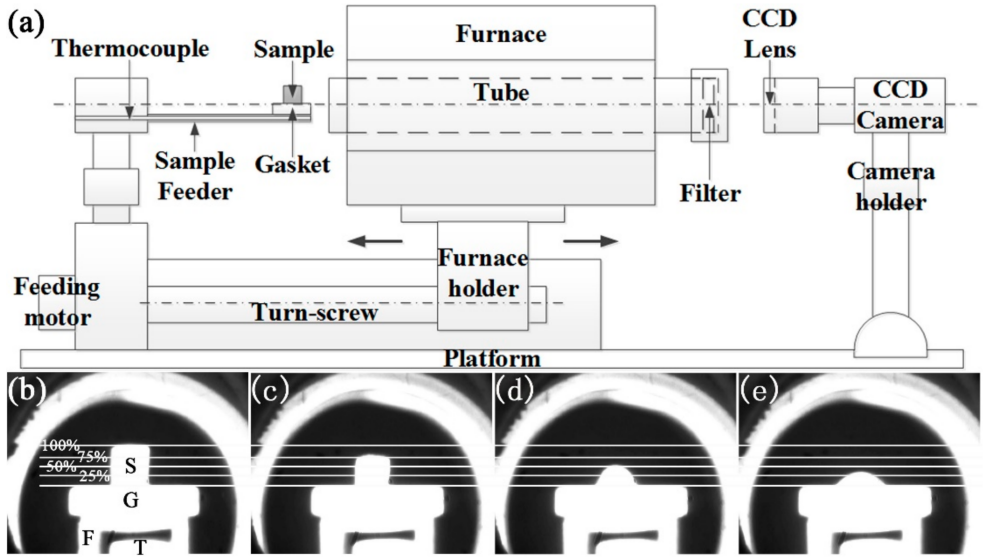


**Figure 1.** (**a**) Schematic diagram of the hot stage microscope and (**b**–**e**) silhouette photographs of samples at various stage. (**b**–**e** are samples with a height of 100%, 75%, 50%, and 35%, respectively). Note: S, G, F, and T in Figure 1b denote the sample, gasket, feeder and thermocouple shown in Figure 1a.

The compositions of samples were analyzed by ICP (ICAP-7400, Thermo Scientific, Waltham, MA, USA), while the total iron and divalent iron contents were measured by titration analysis. X-ray diffraction (XRD) was performed using a Rigaku D/Max 2400 diffractometer (Rigaku, Tokyo, Japan) with Cu Kα radiation (40 kV, 20 mA).

### *2.3. Methods*

The fusion characteristic temperatures were tested as follows. (1) Sample preparation. The nickel slag powder with a particle size of less than 74 μm was mixed with various amounts of CaO to achieve a desired weight percentage. The samples were forced into a mortar to prepare columnar samples with a diameter of 3 mm and height of 3 mm. (2) Temperature testing. First, samples were placed on an alumina gasket, which was located at the edge of the sample feeder. Subsequently, the furnace body was moved in to the limit position so that samples were located in the center of the furnace. This movement can be divided into two stages: a. the furnace was stopped for 60 s after meeting the samples, this place was used for sample drying; b. the furnace was moved again till the end. Finally, samples were heated in air and silhouette photographs (Figure 1b–e) of the samples were recorded by camera when the temperature exceeded 973 K. The first photograph with a sample height of 100% recorded at 973 K (Figure 1b) was defined as the silhouette photograph of the initial sample, while samples with heights of 75%, 50%, and 35% were defined as the softening temperature (*Ts*), hemispherical temperature (*Th*), and fluid temperature (*Tf*), respectively.

The procedure for the oxidization of fayalite in the nickel slag was performed as follows. (1) Different quantities of CaO were added to the water-quenched nickel slag powder and mixed evenly. (2) The mixture was forced into a rectangular alumina boat and placed in the center of the tube in the horizontal furnace. (3) Ar with a flow rate of 1 L/min was used as the purge gas to create an inert atmosphere in the tube for 1 h. (4) Samples were heated to 1658 K (1385 °C) with a heating rate of 5 K/min. (5) The compressed air with a flow rate of 0.1 L/min was injected for different time to oxidize the fayalite in nickel slag. (6) The furnace was purged again by argon with a flow rate of 1 L/min immediately after the specified time while the samples were cooled by furnace.

The magnetic separation processing was introduced in our previous work and performed as follows. (1) The oxidized nickel slag was crushed to powder with a diameter of less than 74 μm and

separated by a magnetic flux density of 300 mT; (2) The magnetic part (Concentrate I) was then crushed into powder with a diameter of less than 50 μm and separated by a magnetic flux density of 300 mT. (3) The iron concentrate was finally obtained after crushing Concentrate II into powder with a diameter of less than 38 μm and separated under a magnetic flux density of 120 mT.

## 3. Results and Discussion

### *3.1. Thermodynamic Analysis*

The relevant reactions in the current work were as follows:

$$Fe_2SiO_{4(s)} = 2FeO_{(s)} + SiO_{2(s)} \quad (1)$$

$$Fe_2SiO_{4(s)} + CaO_{(s)} = 2FeO_{(s)} + CaSiO_{3(s)} \quad (2)$$

$$4FeO_{(s)} + O_{2(g)} = 2Fe_2O_{3(s)} \quad (3)$$

$$6FeO_{(s)} + O_{2(g)} = 2Fe_3O_{4(s)} \quad (4)$$

$$3Fe_2SiO_{4(s)} + O_{2(g)} = 2Fe_3O_{4(s)} + 3SiO_{2(s)} \quad (5)$$

$$4Fe_3O_{4(s)} + O_{2(g)} = 6Fe_2O_{3(s)} \quad (6)$$

$$3Fe_2SiO_{4(s)} + 3CaO_{(s)} + O_{2(g)} = 2Fe_3O_{4(s)} + 3CaSiO_{3(s)} \quad (7)$$

The relationship between $\Delta G^0$ and temperature was established by thermodynamic software FactSage 7.1, and the results were presented in Figure 2. A positive $\Delta G^0$ of Equation (1) means that the decomposition of fayalite cannot take place spontaneously. Conversely, the $\Delta G^0$ of other equations are negative, implying that it is thermodynamically possible for them to occur. FeO can be released from $Fe_2SiO_4$ by the addition of CaO (Equation (2)), and subsequently oxidized to iron oxides (Equations (3) and (4)). Meanwhile, $Fe_2SiO_4$ can be oxidized directly into magnetite ($Fe_3O_4$) (Equation (5)) by $O_2$, but the tendency will much stronger if CaO is present (Equation (7)). Although $Fe_3O_4$ can be oxidized to $Fe_2O_3$, as shown in Equation (6), the tendency is weaker than that of Equation (4). Thus, the addition of CaO is expected to promote the reaction between $Fe_2SiO_4$ and $O_2$ to produce $Fe_3O_4$.

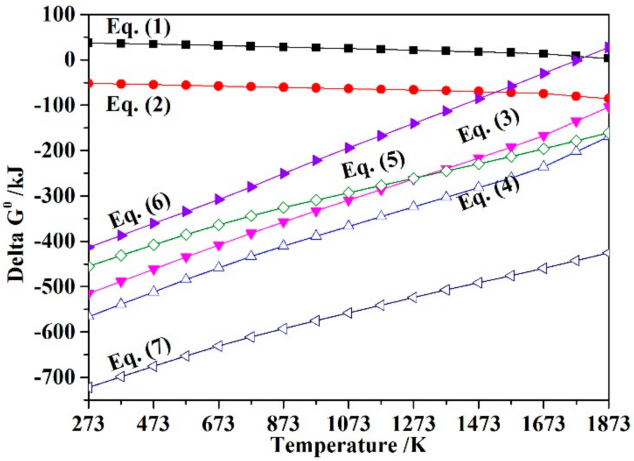


**Figure 2.** Relationship between $\Delta G^0$ and temperature.

Although the addition of CaO is thermodynamically beneficial for the reaction between fayalite and oxygen, how it works in the system was still unknown. Thus, to understand the role of CaO in the oxidization of fayalite in nickel slags, a series of phase diagrams were drawn, as shown in Figure 3, it can be found that the addition of CaO can significantly affect the phase components and liquidus temperature.

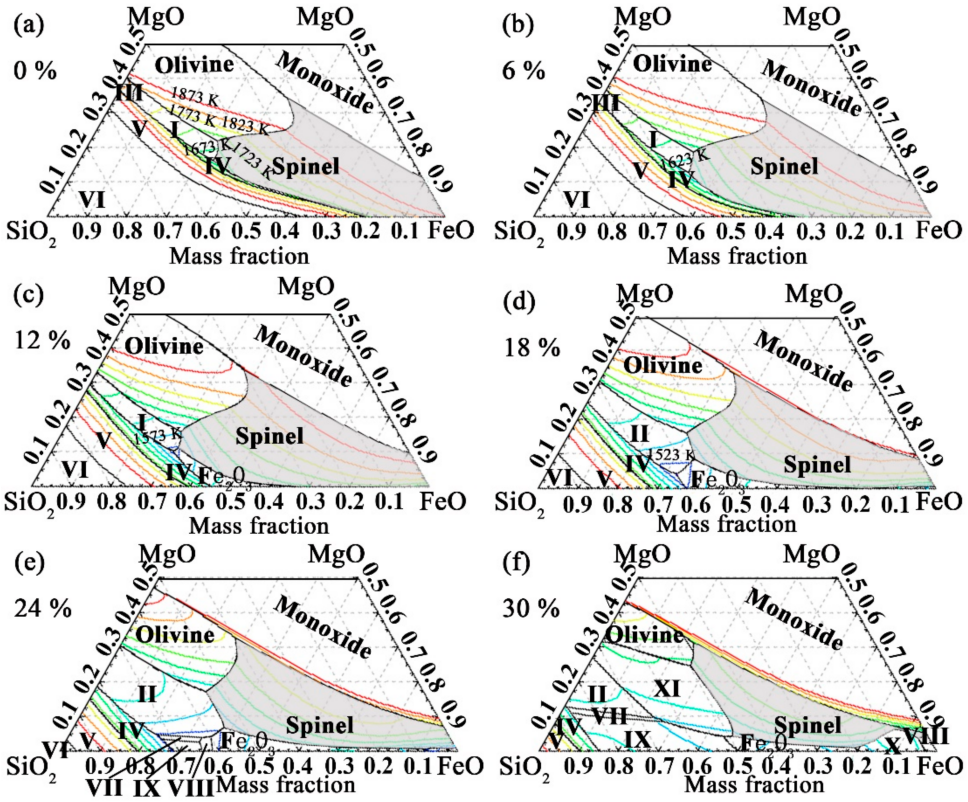


**Figure 3.** Effects of CaO addition on the phase diagram of FeO-$SiO_2$-MgO-CaO slag in an air atmosphere. (I–XI represents orthopyroxene, clinopyroxene, protopyroxene, $SiO_2$ (s4), $SiO_2$ (s6), Liquid Slag, wollastonite, $Ca_2Fe_2O_5$ (s), $CaSiO_3$ (s2), $Ca_2SiO_4$, and melilite, respectively). (**a**–**f**): *w*(CaO) was specified as 0 wt.%, 6 wt.%, 12 wt.%, 24 wt.%, and 30 wt.%, respectively.

Spinel ($(Fe,Mg)Fe_2O_4$), which is a solid solution of magnetite ($Fe_3O_4$) and magnesium ferrite ($MgFe_2O_4$) when $Mg^{2+}$ partially substitutes for $Fe^{2+}$ sites in the structure, is marked with gray and is the major iron-bearing phase if the CaO content is less than 6 wt.%. Hematite ($Fe_2O_3$) will appear when the MgO content is less than 10 wt.% and its area grows with the increase of the CaO content between 12 and 24 wt.%. The phase compositions are much more complicated in this range. Furthermore, melilite ($Ca_2MgSi_2O_7$) will form if the CaO content increases to 30 wt.%. It is worthwhile to mention that the spinel area increased at 6 wt.% CaO when compared with 0 wt.% CaO. However, it decreased with the increasing of the CaO content. The olivine area also decreased significantly with the increasing of the CaO content.

The liquidus temperature changes with the addition of CaO. If no CaO is present, there is only a long and narrow liquid phase zone below 1873 K, while the lowest liquidus temperature is 1673 K. However, it expands and moves towards the $SiO_2$ corner of the phase diagram with the addition of CaO. A new liquid phase zone at 1623 K forms at the intersection of the spinel, pyroxene and $SiO_2$ regions when the CaO content is 6 wt.%. In addition, if the CaO content increases to 12 wt.%, the liquid zone below 1873 K expands and two other liquid phase zones forms at 1573 K and 1523 K. However, the liquid phase zone, with the lowest liquid temperature, begins to move toward the hematite phase zone at 18 wt.% CaO. Finally, the liquid phase zone, that is 1523 K, disappeared at 30 wt.% CaO, while the liquid zone of 1573 K expands when the MgO content is less than 20 wt.%.

### *3.2. Fusion Characteristic Temperatures*

As mentioned above, the liquidus temperature of nickel slag can be affected by the addition of CaO. Thus, it is necessary to investigate how the CaO affects the temperature. Because FactSage can be used for the prediction of phase evolution in various slag systems [16], and HSM was also used to

measure the fusion temperatures [17–19]. Thus, both theoretical calculations and experiments were used for the investigations.

The effects of CaO content on the fusion characteristic temperatures, i.e., the softening temperature (*Ts*), hemispherical temperature (*Th*), and fluid temperature (*Tf*), of the synthetic slags, nickel raw slags and the calculated phase components at solidus temperature are shown in Figure 4. The characteristic temperatures of the synthetic slags and water-quenched nickel slag can be significantly influenced by the addition of CaO. For the synthetic slags, the fusion characteristic temperature first decreased and subsequently increased with increasing CaO content (Figure 4a). The inflection points of *Ts*, *Th*, and *Tf* were 1463 K, 1475 K, and 1486 K, corresponding to a CaO content of 12%, 12%, and 18%, respectively. Similar variations can also be found in the nickel slags when compared with the synthetic slags (Figure 4b). The same tendency was found for the solidus temperatures of samples when the inflection point was 1497 K at 6 wt.% CaO (Figure 4c).

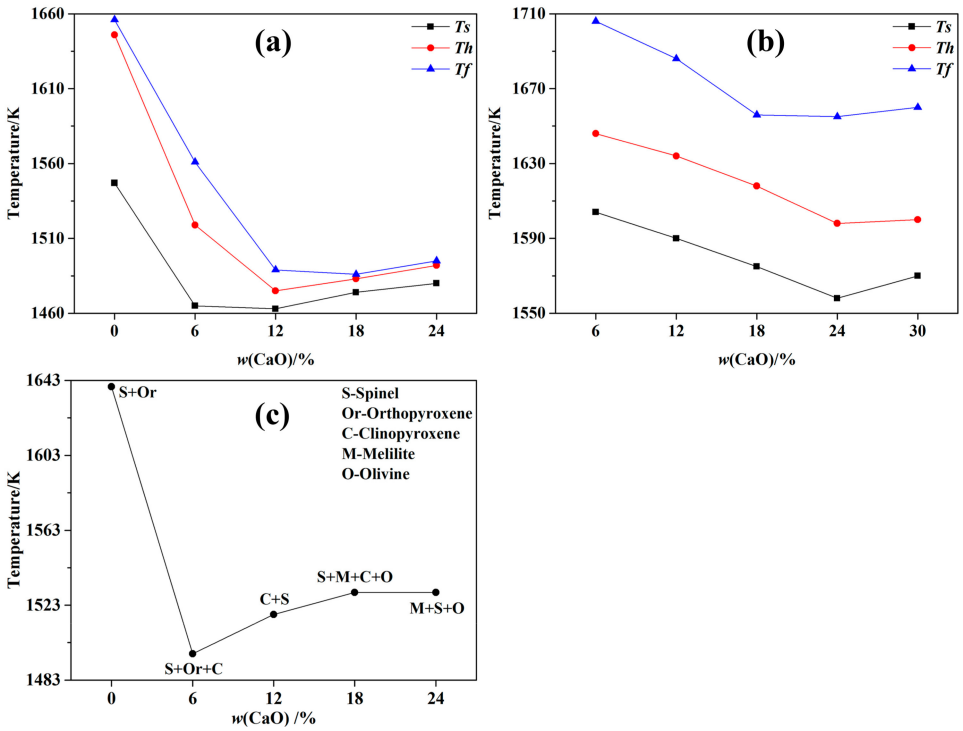


**Figure 4.** Effects of $w$(CaO) on fusion characteristic temperatures of the (**a**) synthetic slags, (**b**) nickel slags, and (**c**) calculated phase compositions at solidus temperature.

The reduction of the fusion characteristic temperatures was mainly caused by the variation of phase components at the solidus temperature, which is illustrated in Figure 4c. If CaO was not added, protopyroxene, with a high melting temperature, would have formed. The fusion temperatures were significantly decreased when clinopyroxene was formed at higher CaO contents. However, the fusion temperatures increased with increasing CaO content when a new high melting phase, melilite, was formed. Thus, an appropriate addition of CaO is beneficial for the reducing of the fusion characteristic temperatures by influencing the phase components.

### 3.3. Oxidation of Fayalite

The phase diagram shown in Figure 3 indicates that the phase components can also be affected by the addition of CaO. Thus, the influence of CaO addition on the oxidization of fayalite was investigated by theoretical calculations and experiments.

Slags, some polymers in the form of chains or rings, consist of $SiO_4^{4-}$ tetrahedral units with each $Si^{4+}$ surrounded (tetrahedrally) by $4O^{2-}$ ions [20]. Theoretically, pyroxene will form along

with the released oxygen ion when the nesosilicates polymerized under oxygen-deficient conditions (Equation (8)).

$$SiO_4^{4-} + SiO_4^{4-} = Si_2O_6^{4-} + 2O^{2-} \quad (8)$$

The CaO acts as an $O^{2-}$ ion donor [21], as shown in Equation (9):

$$CaO = Ca^{2+} + O^{2-} \quad (9)$$

In addition, the reaction between $Fe_2SiO_4$ and $O_2$ can be enhanced by CaO through the destruction of the structure of fayalite ($Fe_2SiO_4$) to release FeO, which can then react with oxygen ions as well as the injected $O_2$ to produce magnetite ($Fe_3O_4$).

The melting temperature of magnetite ($Fe_3O_4$), which is as high as 1871 K, allows it to crystalize first from the liquid slag. Meanwhile, due to the similar properties of $Mg^{2+}$ and $Fe^{2+}$, $Mg^{2+}$ can partially substitute for $Fe^{2+}$ at the $Fe_3O_4$ sites in the structure and thus a solid solution of magnetite and magnesium ferrite ($MgFe_2O_4$) forms, and the formation of hematite ($Fe_2O_3$) may be hindered. Similar results can also be found in Semykina's study of the oxidization of FeO-CaO-$SiO_2$ slag and FeO-MnO-CaO-$SiO_2$ slags [14,15], where hematite can be found in the products of the former but cannot found in the latter when magnetite/manganese ferrite forms. However, an explanation of this phenomenon was not presented. Thus, we propose the following explanation.

Because the equilibrium constant of Equation (2) can be expressed as

$$K_2 = \frac{a(FeO)}{a(CaO)} \quad (10)$$

where $a$(FeO) and $a$(CaO) represents the activity of FeO and CaO, respectively.

As we known, the equilibrium constant $K$ is a function of temperature and only changes when the temperature is changed. Therefore, the addition of CaO increases the $a$(CaO) and lead to an increase of $a$(FeO) at a given temperature to shift the reaction toward the products on the right of Equation (2).

Equation (4) can occur more easily than Equation (3), and there may be some hematite produced. However, the generated $Fe_2O_3$ can react with FeO to produce $Fe_3O_4$, which can be shown as follows:

$$Fe_2O_3 + FeO = Fe_3O_4 \quad (11)$$

where the equilibrium constant $K$ can be written as

$$K_{10} = \frac{1}{a(FeO) \cdot a(Fe_2O_3)} \quad (12)$$

where $a$(FeO) and $a$($Fe_2O_3$) represents the activity of FeO and $Fe_2O_3$, respectively.

The increased $a$(FeO) may decrease the $a$($Fe_2O_3$) and thus more $Fe_3O_4$ can be generated. Moreover, MgO can also react with $Fe_2O_3$ to form $MgFe_2O_4$ as follows:

$$MgO + Fe_2O_3 = MgFe_2O_4 \quad (13)$$

where the equilibrium constant can be written

$$K_{11} = \frac{1}{a(MgO) \cdot a(Fe_2O_3)} \quad (14)$$

where $a$(MgO) and $a$($Fe_2O_3$) represents the activity of MgO and $Fe_2O_3$, respectively.

Therefore, the forward reaction of Equation (11) was caused by the decrease of $a$($Fe_2O_3$) to produce $MgFe_2O_4$. In short, the addition of CaO can not only promote the decomposition of $Fe_2SiO_4$ but also hinders the formation of $Fe_2O_3$.

To confirm this, nickel slag mixed with various CaO contents was then oxidized by compressed air with a flow rate of 300 mL/min after heating in an Ar atmosphere. As shown in Figure 5a, the divalent iron content ($w(Fe^{2+})$) decreases with increasing CaO content in the range of 6 to 24 wt.%. Conversely, an increasing $w(Fe^{3+})/w(Fe^{2+})$ implies that the trivalent iron content ($w(Fe^{3+})$) increases. Noting that the oxidation rate at various CaO contents were different. The $w(Fe^{2+})$ with a CaO content less than 18 wt.% decreased rapidly before being oxidized for 60 min, but that of 24 wt.% CaO was steady after oxidation for 40 min. A similar phenomenon can also be found in the variation of the $w(Fe^{3+})/w(Fe^{2+})$. The implication is that the oxidation rate of fayalite in nickel slag can be accelerated by a moderate content of CaO.

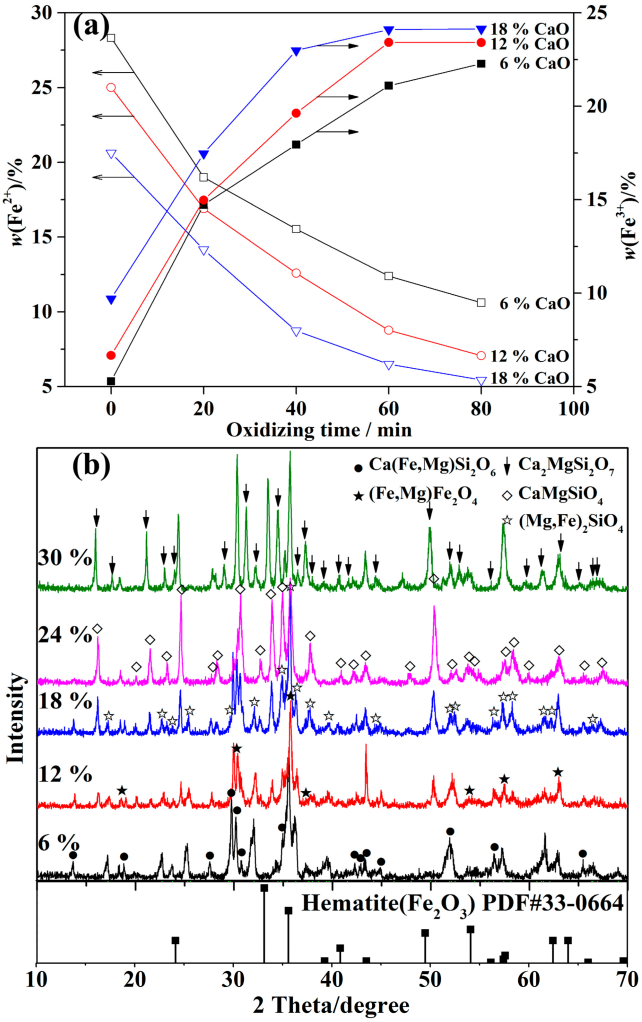


**Figure 5.** (**a**) Effects of CaO content on the iron state variation and (**b**) X-ray diffraction (XRD) patterns of samples.

The XRD patterns in Figure 5b showed that hematite ($Fe_2O_3$) was still not observed after oxidizing for 100 min even though the $Fe^{3+}/Fe^{2+}$ ratio was greater than 2, which is the theoretical ratio of $Fe^{3+}/Fe^{2+}$ in $Fe_3O_4$. As mentioned in Section 3.1, several kinds of calcium silicates can form during the oxidization of FeO-$SiO_2$-MgO-CaO slag in an air atmosphere. However, it was proved by the XRD patterns shown in Figure 5b that the silicates mainly consisted of augite ($Ca(Fe,Mg)Si_2O_6$), monticellite ($CaMgSiO_4$), and akermanite ($Ca_2MgSi_2O_7$). It is worthwhile to note that the peaks of forsterite ($Mg_2SiO_4$) weakened and finally disappeared in the XRD patterns when the CaO content was above 18 wt.%, while peaks of monticellite strengthened. Moreover, akermanite was found only when the CaO content was at 30 wt.%.

Thus, the addition of CaO accelerates the oxidization of fayalite in nickel slag to generate magnetite, but CaO addition to more than 12 wt.% may influence the phase components significantly rather than the oxidization of fayalite.

### *3.4. Crystallization Processing*

Because spinel phases ($(Fe,Mg)Fe_2O_4$) were the dominant iron-bearing phases in the oxidation products, the effects of CaO addition on the crystallization were calculated by FactSage 7.1. The mass proportion of the crystalized spinel phases with various CaO contents at temperatures above 1658 K are shown in Figure 6a. From which we can found that the crystalized spinel phases were reduced with the increasing CaO content. This was mainly due to the following two reasons. The increasing CaO content led to a lower absolute percentage of spinel phases when more complicated calcium silicates were formed. Meanwhile, the crystallization temperature of the spinel phases, which was significantly affected by the increasing CaO content, shown in Figure 6b also played a significantly role. If spinel phases can be crystalized at a higher temperature and lower CaO content, the crystal nuclei can form earlier and have a larger temperature gradient at 1658 K, which is beneficial for the crystallization of spinel. Conversely, the crystal nuclei formed at higher CaO contents have a relative smaller temperature gradient.

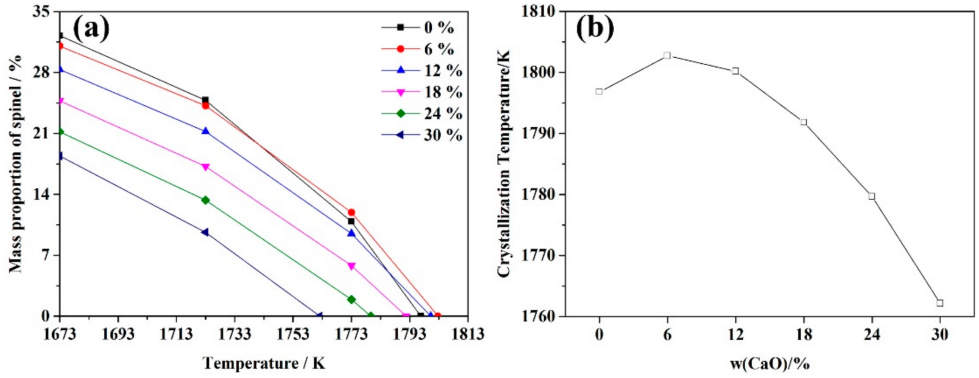


**Figure 6.** Effects of CaO content on the (**a**) mass proportion of spinel phase above 1673 K and (**b**) crystallization temperature of spinel phases.

### *3.5. Magnetic Separation*

As mentioned in Section 3.3, the excess addition of CaO has no effect on the oxidization of fayalite, but the phase components, especially the silicates, can be influenced significantly. Because magnetite and magnesium ferrite were the dominant iron-containing phases in the oxidized nickel slag, magnetic separation was performed to separate these magnetic minerals. As presented in Figure 7, the recovery rate and yield of iron were first increased and later decreased as the CaO increased, while the iron content remained nearly constant. It is also worthwhile to mention that the maximum value of the iron recovery rate and yield achieved were 74.71% and 54.09% at 12 wt.% CaO, while the iron content was 54.13%.

The XRD patterns of the magnetically separated products are shown in Figure 8. Magnetite and magnesium ferrite are the dominant phases in the iron concentrate (Figure 8a), though some silicates with weaker peaks were also observed. Conversely, the tailing slag consisted of augite ($Ca(Fe,Mg)Si_2O_6$), monticellite ($CaMgSiO_4$), and wollastonite ($CaSiO_3$), and the peaks of these silicates were much stronger than those of magnetite and magnesium ferrite. Furthermore, the compositions of the iron concentrate and tailing slag shown in Table 2 also indicate that iron is the major element in the concentrate but not in tailing slag, while Si, Mg, and Ca are rich in the tailing slag but rare in the concentrate. As discussed above, a CaO content of 12 wt.% was beneficial for the iron recycling from nickel slags by oxidation-magnetic separation.

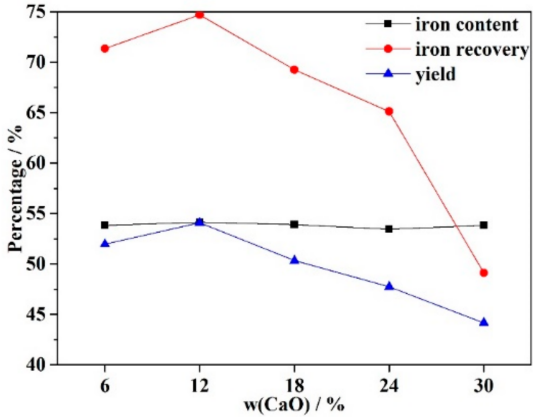


**Figure 7.** Effects of CaO content on the iron content, recovery rate, and yield of concentrate.

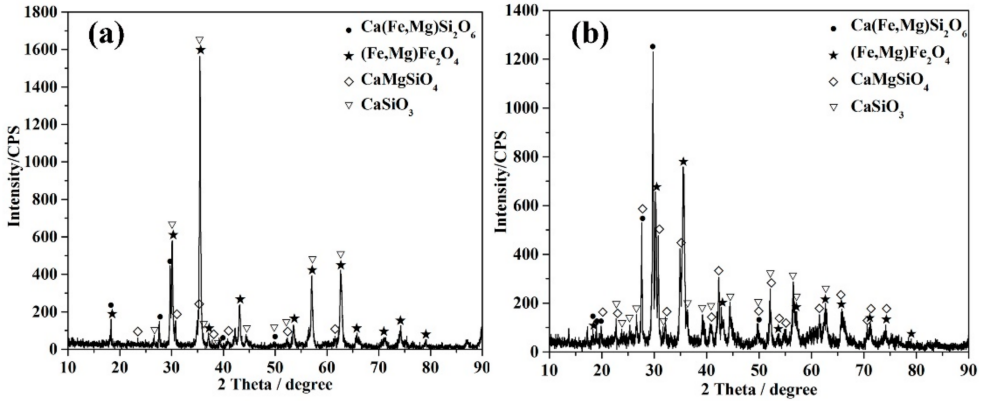


**Figure 8.** XRD patterns of the (**a**) separated iron concentrate and (**b**) tailing slag of the oxidized nickel slag at 12 wt.% CaO.

**Table 2.** Components of the separated concentrate and tailing slag (wt.%).

| Products | TFe | Si | Mg | Ca | Ni | Co | Cu | Pb | Zn | As |
|---|---|---|---|---|---|---|---|---|---|---|
| Iron concentrate | 54.13 | 4.96 | 3.28 | 0.79 | 0.22 | 0.13 | 0.26 | 0.006 | 0.047 | 0.001 |
| Tailing slag | 19.60 | 21.36 | 5.48 | 7.16 | 0.08 | 0.06 | 0.12 | 0.015 | 0.050 | 0.001 |

## 4. Conclusions

The effects of CaO on the iron recycling from nickel slags by oxidization-magnetic separation were investigated in this study. The findings of this work are summarized as follows:

1. Thermodynamic analysis proved that $Fe_2SiO_4$ cannot decompose spontaneously, but the addition of CaO plays a positive role in the oxidization of fayalite in nickel slag to produce magnetite. Diagrams of FeO-$SiO_2$-MgO-CaO slag in an air atmosphere drawn by FactSage 7.1 showed that the phase components, as well as the area of spinel phase, can be affected by the addition of CaO.
2. With the increase of CaO content, the fusion characteristic temperatures decreased rapidly until a CaO content of 12 wt.% and then slightly increased. This was mainly caused by the variation of phase components at various CaO contents.
3. Experiments proved that the oxidization of $Fe_2SiO_4$ in nickel slags can be accelerated significantly by the addition of CaO. Due to the addition of CaO, $a$(FeO) increased and thus led to a decrease of $a$($Fe_2O_3$), which promotes the reaction between MgO and $Fe_2O_3$ to form $MgFe_2O_4$. However, excess addition of CaO only formed more silicates.
4. The crystallization temperature can be reduced by the increasing CaO content. As the CaO content increased, the crystallization temperature decreased, and fewer spinel crystals formed.

5. The recovery rate and yield of iron were first increased and later decreased as the CaO increased, while the iron content remained nearly constant. XRD patterns showed that magnetite and magnesium ferrite were the dominant phases in the iron concentrate, while the tailing slag mainly consisted of several silicates. Ultimately, the maximum iron recovery and yield of concentrate achieved were 74.71% and 54.09%, while the iron content was 54.13%.

**Author Contributions:** Conceptualization, Y.M. and X.D.; Methodology, Y.M.; Software, Y.M.; Validation, X.D.; Formal Analysis, Y.M.; Investigation, Y.M.; Resources, X.D.; Data Curation, Y.M.; Writing—Original Draft Preparation, Y.M.; Writing—Review and Editing, X.D.; Visualization, Y.M.; Supervision, X.D.; Project Administration, X.D.; Funding Acquisition, X.D.

**Funding:** This research was funded by the Science and Technology Major Project Plan of Gansu Province.

**Acknowledgments:** The authors wish to thank the Jinchuan Group Co., Ltd., China, for supplying the nickel slags used in this work.

**Conflicts of Interest:** The authors declare no conflict of interest. The funders had no role in the design of the study; in the collection, analyses, or interpretation of data; in the writing of the manuscript, or in the decision to publish the results.

## References

1. Zhao, J.X.; Zhao, Z.Y.; Cui, Y.R.; Shi, R.M.; Tang, W.D.; Li, X.M.; Shang, N. New slag for nickel matte smelting process and subsequent Fe extraction. *Metall. Mater. Trans. B* **2018**, *49*, 304–310. [CrossRef]
2. Wolf, A.; Mitrašinović, A.M. Nickel, copper and cobalt coalescence in copper cliff converter slag. *J. Min. Metall. Sect. B* **2016**, *52*, 143–150. [CrossRef]
3. Li, Y.J.; Papangelakis, V.G.; Perederiy, I. High pressure oxidative acid leaching of nickel smelter slag: Characterization of feed and residue. *Hydrometallurgy* **2009**, *97*, 185–193. [CrossRef]
4. Krogerus, E.V.; Talonen, T.T. Method for Continuous Reduction of Molten Metallurgical Slag in an Electric Furnace. U.S. Patent 4,737,186, 12 April 1988.
5. Ma, Y.B.; Du, X.Y.; Shen, Y.Y.; Li, G.Z.; Li, M. Crystallization and beneficiation of magnetite for iron recycling from nickel slags by oxidation-magnetic separation. *Metals* **2017**, *7*, 321–332. [CrossRef]
6. Zhao, J.X.; Cui, Y.R.; Gao, X.T.; Lu, X.T.; Tang, W.R.; Li, X.M.; Shi, R.M. Method for Smelting Nickel-Copper from Sulfide Ores by Virtue of Pyrogenic Process and Extracting Iron. CN. Patent 201410376672, 30 March 2016.
7. Hao, W.Y. Comprehensive utilization of the smelting slags in Jinchuan. *Gansu Metall.* **1995**, *2*, 23–27.
8. Ducret, A.C.; Rankin, W.J. Liquidus temperatures and viscosities of FeO-$Fe_2O_3$-$SiO_2$-CaO-MgO slags at compositions relevant to nickel matte smelting. *Scand. J. Metall.* **2002**, *31*, 59–67. [CrossRef]
9. Fujino, K.; Murakami, T.; Kasai, E. Effect of addition of CaO component on the oxidation reaction of wustite particles in sintering bed. *ISIJ Int.* **2015**, *55*, 940–946. [CrossRef]
10. Mackwell, S.J. Oxidation kinetics of fayalite ($Fe_2SiO_4$). *Phys. Chem. Miner.* **1992**, *19*, 220–228. [CrossRef]
11. Semykina, A.; Shatokha, V.; Iwase, M.; Seetharaman, S. Kinetics of oxidation of divalent iron to trivalent state in liquid FeO-CaO-$SiO_2$ slags. *Metall. Mater. Trans. B* **2010**, *41*, 1230–1239. [CrossRef]
12. Semykina, A. The kinetics of oxidation of liquid FeO-MnO-CaO-$SiO_2$ slags in air. *Metall. Mater. Trans. B* **2012**, *43*, 56–63. [CrossRef]
13. Heo, J.H.; Park, S.S.; Park, J.H. Effect of slag composition on the distribution behavior of Pb between $Fe_t$O-$SiO_2$(-CaO, $Al_2O_3$) slag and molten copper. *Metall. Mater. Trans. B* **2012**, *43*, 1098–1105. [CrossRef]
14. Heo, J.H.; Kim, B.S.; Park, J.H. Effect of CaO addition on iron recovery from copper smelting slags by solid carbon. *Metall. Mater. Trans. B* **2013**, *44*, 1352–1363. [CrossRef]
15. Zhao, Z.L.; Tang, H.Q.; Guo, Z.C. Effects of CaO on precipitation morphology of metallic iron in reduction of iron oxides under CO atmosphere. *J. Iron Steel Res. Int.* **2013**, *20*, 16–24. [CrossRef]
16. Chen, M.; Zhang, W.D.; Zhao, Z.X.; Wang, D.Q.; Evans, T.; Zhao, B.J. High temperature softening behaviours of iron blast furnace feeds and their correlations to the microstructures. In *The 6th International Symposium on High-Temperature Metallurgical Processing*; Jiang, T., Hwang, J.-Y., Eds.; Springer: Cham, Switzerland, 2016; pp. 67–74.

17. Yu, Y.; Wang, D.; Li, J.L.; Zhu, H.Y.; Xue, Z.L. Thermodynamic calculation of FeO effect on precipitation of spinel containing chromium in CaO-$SiO_2$-MgO-$Al_2O_3$-$Cr_2O_3$ system. *J. Wuhan Uni. Sci. Technol.* **2018**, *41*, 15–19. [CrossRef]
18. Sagadin, C.; Luidold, S.; Wagner, C.; Wenzl, C. Melting behaviour of ferronickel slags. *JOM* **2016**, *68*, 3022–3028. [CrossRef]
19. Talapaneni, T.; Yedla, N.; Sarkar, S.; Pal, S. Effect of Basicity, $Al_2O_3$ and MgO content on the softening and melting properties of the CaO-MgO-$SiO_2$-$Al_2O_3$ high alumina quaternary slag system. *Metall. Res. Technol.* **2016**, *113*, 501–511. [CrossRef]
20. Seetharaman, S. *Fundamentals of Metallurgy*; Woodhead Publishing Limited: Abington, UK, 2005; pp. 115–116.
21. Wang, L.; Zhang, C.; Cai, D.X.; Zhang, J.Q.; Sasaki, Y.; Ostrovski, O. Effects of CaO/$SiO_2$ ratio and $Na_2O$ content on melting properties and viscosity of $SiO_2$-CaO-$Al_2O_3$-$B_2O_3$-$Na_2O$ mold fluxes. *Metall. Mater. Trans. B* **2017**, *48*, 516–526. [CrossRef]